RESEARCH ARTICLE
SPACE PHYSICS: MAGNETOSPHERIC PHYSICS

Earth and Planetary Physics
1: 35-43, 2017
doi: 10.26464/epp2017005

Correlations between plasmapause evolutions and auroral signatures during substorms observed by Chang'e-3 EUV Camera

XiaoXin Zhang[1], Fei He[2,3*], Bo Chen[4], Chao Shen[5], and HuaNing Wang[6]

[1]Key Laboratory of Space Weather, National Center for Space Weather, China Meteorological Administration, Beijing 100081, China;
[2]Key Laboratory of Earth and Planetary Physics, Institute of Geology and Geophysics, Chinese Academy of Sciences, Beijing 100029, China;
[3]College of Earth Sciences, University of Chinese Academy of Sciences, Beijing 100049, China;
[4]Changchun Institute of Optics, Fine Mechanics and Physics, Chinese Academy of Sciences, Changchun 130033, China;
[5]School of Natural Sciences and Humanity, Harbin Institute of Technology Shenzhen Graduate School, Shenzhen 518005, China;
[6]National Astronomical Observatories, Chinese Academy of Sciences, Beijing 100012, China

Abstract: The plasmapause locations determined from the Chang'e-3 (CE-3) Extreme Ultraviolet Camera (EUVC) images and the auroral boundaries determined from the Defense Meteorological Satellite Program (DMSP) Special Sensor Ultraviolet Spectrographic Imager (SSUSI) images are used to investigate the plasmaspheric evolutions during substorms. The most important finding is a nightside pointing plasmaspheric plume observed at 23:05 UT on 21 April 2014 under quiet solar wind and geomagnetic conditions, which drifted from the dusk sector. High correlations between the plasmapause evolutions and the auroral signatures exist during substorms. After substorm onset, the plasmapause erosion and the equatorward expansion of the auroral oval occur almost simultaneously in both MLT and UT, and then both the erosion and the expansion propagate westward and eastward. It is suggested that the plasmaspheric erosion and its MLT propagations are induced by the enhanced earthward plasma convection during substorm period, and the substorm dipolarization causes pitch-angle scattering of plasma sheet electrons and the resulting precipitation excites aurora emissions at the same time.

Keywords: Plasmasphere; Chang'e-3; EUVC; Minimum *L* Algorithm; Substorm

Citation: Zhang, X. X., F. He, B. Chen, C. Shen, and H. N. Wang (2017). Correlations between plasmapause evolutions and auroral signatures during substorms observed by Chang'e-3 EUV Camera. *Earth Planet. Phys.*, *1*, 35-43. http://doi.org/10.26464/epp2017005

1. Introduction

The ionosphere-originated cold and dense plasma region in the plasmasphere is the core region of inner magnetospheric couplings (Lemaire et al., 1998). The plasmaspheric responses to storms/substorms that are triggered by the changes of solar wind and interplanetary magnetic field (SW-IMF) have always been a hot topic in the inner magnetospheric research. Numerous investigations of IMAGE Extreme Ultraviolet (EUV) images (Sandel et al., 2000; Burch, 2003) have revealed that changes in SW-IMF parameters can cause the erosion or refilling of the plasmasphere (Sandel et al., 2001, 2003; Spasojević et al., 2003; Goldstein et al., 2003a, 2005; He F et al., 2012a, 2013). Plume is a typical global structure of the plasmasphere under disturbed SW-IMF conditions and in storm times, which can be generally formed in the post-noon to dusk sector as predicted by numerical modeling (Grebowsky, 1970; Chen AJ and Wolf, 1972; Chen AJ and Grebowsky, 1974; Rasmussen et al., 1993; Ober et al., 1997a; Pierrard and Lemaire, 2004) and observed by IMAGE mission (Sandel et al., 2001; Spasojević et al., 2003, 2004; Goldstein et al., 2003a, b, 2004; He F et al., 2013), Cluster (Darrouzet et al., 2008, 2009), CRRES (Moldwin et al., 2004), LANL (Goldstein et al., 2014), and THEMIS (Walsh et al., 2014). Most of the previous works have focused on the study of the plasmaspheric evolutions under strongly disturbed SW-IMF or geomagnetic conditions. During disturbed times, however, the variations of the SW-IMF and the geomagnetic conditions are so complicated that one cannot clearly distinguish which physical process (external or internal) contributes more to the dynamics of the plasmasphere. It is also known that the plasmapause can move toward the Earth during substorm times and substorms may play an important role in the plasmaspheric dynamics (Kwon et al., 2015; He F et al., 2016). On the other hand, the evolutions of the plasmaspheric structures under quiet SW-IMF and/or geomagnetic conditions have not been fully understood yet. The observation of nightside pointing plume during quiet and less disturbed SW-IMF and geomagnetic conditions has been seldom reported in the literature (Grebowsky, 1970; Ober et al., 1997b).

In addition to the external trigging factors (e.g., SW-IMF), dynamics of the inner magnetosphere (the ring current and radiation belts) and the ionosphere can also impact the evolutions of the plasmasphere. One important signature of the inner magnetosphere is the auroral substorm due to the strong ion and electron precipitations in the ionosphere (Akasofu, 1964). In the substorm

Correspondence to: F. He, hefei@mail.iggcas.ac.cn
Received 10 APR 2017; Accepted 06 JUL 2017.
Accepted article online 17 AUG 2018.

onset phase, the aurora intensifies suddenly and moves equatorward and poleward in the premidnight magnetic local time (MLT) (McPherron et al., 1973). The front of the dipolar magnetic field (the so-called "dipolarization front") moves towards the Earth during the substorms, allowing more magnetotail plasma energized and transported into the polar ionosphere and the auroral oval expanded more equatorward (Goldstein et al., 2007; Runov et al., 2009; Ge YS et al., 2012). The strong sunward compression by the substorm dipolarization front also causes the earthward moving of the nightside plasmasphere (Carpenter and Smith, 2001).

The auroral brightening and expansion are the general form of substorm activity which reflects the dynamic of the inner magnetosphere and ionosphere, such as magnetotail dipolarization, particle injection, and particle precipitation. A big collection of global images obtained from the Defense Meteorological Satellite Program (DMSP) Special Sensor Ultraviolet Spectrographic Imager (SSUSI) (Paxton et al., 1992) can be used to study the auroral substorm activities. Additionally, the Chang'e-3 (CE-3) Extreme Ultraviolet Camera (EUVC) landed on the lunar surface is used to image the global plasmasphere at 30.4 nm from side perspectives with a field of view of 15°, an angular resolution of 0.1° and a temporal resolution of 10 min (Chen B et al., 2014; Feng JQ et al., 2014; Yan Y et al., 2016; He F et al., 2016), and provides us an opportunity to study the global plasmaspheric evolutions during substorms. In this investigation, EUVC and SSUSI data obtained under relatively weak and steady SW-IMF conditions on 21 February and 21 April 2014 will be used to study the relationships between global plasmaspheric evolution and the substorm activities.

Note that the evolutions of the plasmasphere during substorms were investigated with a focus on the variations of the plasmapause at noon and it was inferred that there may be a causal relationship between the substorms and the formation of the plasmaspheric bulges in a previous work (He H et al., 2016). In this investigation, we will explore the global evolution of plasmasphere and its correlation with the auroral signature during substorms.

2. Overview of SW-IMF and Geomagnetic Conditions

The SW-IMF and geomagnetic conditions on 21 February 2014 (Case I, in red) and on 21 April 2014 (Case II, in blue) are shown in Figure 1, with time shift of 45 min from ACE's location to the dayside magnetopause (the propagation of solar wind is calculated with the method in (Zhang XX et al., 2005)). Case I shows that the magnetosphere was recovering from the moderate geomagnetic storm happened on 19 February, associated with *Dst* around -50 nT and *Kp* below 3.0. Figure 1b indicates a southward turning of IMF happened at approximately 03:52 UT and lasted until the end of the day. After 04:00 UT, both SW-IMF and geomagnetic conditions were steady, with the amplitudes of B_y and B_z both below 5 nT, V_{SW} around 500 km/s, and N_{SW} below 2 cm^{-3}. It can be seen in Figures 1e and 1f that the auroral geomagnetic activity was disturbed after ~ 07:00 UT, as indicated by the *AE* index, during the recovery phase of the moderate storm in which the solar-wind-driven convection (E_{SW} < 2 mV/m) was weak.

Figures 1f-1h show that the magnetosphere had several substorms for Case II, in which B_z turned to south at ~ 01:00 UT and then was back to north at ~ 03:00 UT until ~ 08:00 UT when it turned to south again and continued for ~ 8 hours as indicated in Figure 1b. While as shown in Figures 1c and 1d, there were significant increases in N_{SW} and slow decreases in V_{SW} during these two periods of southward IMF, respectively. The magnetosphere was in a weak solar-wind-driven convection (E_{SW} < 3 mV/m) as indicated in Figure 1e.

3. Overview of Plasmaspheric Evolutions Seen by EUVC

The EUVC images and the corresponding plasmapause locations determined from the EUVC images using the Minimum *L* Algorithm (MLA) (He F et al., 2011, 2012b, 2016) are shown in Figure 2 and Figure 3 in 2-hour intervals for Case I and Case II, respectively.

The MLA is a line of sight (LOS) tracing algorithm first proposed to determine the plasmapause locations from the IMAGE EUV images (Wang CL et al., 2007). In optical imaging of the plasmasphere, each pixel in the image represents a specific LOS in space and the intensity is proportional to the column integrated He^+ density along the LOS. For the pixels at the sharp boundary in a plasmaspheric image, the corresponding LOS's are assumed to be tangential to the plasmapause. When the points in the LOS are traced on the magnetic equatorial plane along magnetic field lines, the one with minimum *L*-value is determined to be the plasmapause. The MLA has been validated in application to plasmaspheric images obtained in an Earth's polar-orbiting imager (e.g., IMAGE EUV) and the MLT dependence of the plasmapause locations can be determined since the images are approximately projected onto the magnetic equatorial plane. Then the MLA was further developed (He F et al., 2011, 2016) to be applied to the plasmaspheric images obtained in side perspectives (e.g., CE-3 EUVC). The plasmapause locations determined from the CE-3 EUVC images via MLA has been validated with in situ observations from the Defense Meteorological Satellite Program (DMSP), the Time History of Events and Macroscale Interactions during Substorms (THEMIS), and the Van Allen Probes (VAP) at different MLTs (He F et al., 2016). Excellent agreement between the determined plasmapauses seen by EUVC and other satellites indicates the reliability of the data as well as the MLA.

In determination of the plasmapause locations in the equatorial plane of the solar magnetic (SM) coordinate system, the MLA is realized through the following steps (He F et al., 2016).

The first step is to calculate the transformation matrixes between the satellite coordinate system (SCS) and SM based on the unit vectors of the *x*, *y*, and *z* axes of SCS in SM coordinate system given in the header of EUVC data files.

The second step is to automatically extract the plasmaspheric outline pixels defined by the outermost sharp edge where the brightness of 30.4 nm He^+ emissions drops more than 1 order of magnitude in the radial directions in the EUVC images. Then the pixels are manually checked to ensure that the pixels are located at true plasmapause outline since in some times the noise comes from the contamination by sunlight might mislead the automatic processing procedure. This is necessary to ensure the determined plasmapause locations to be correct and reliable. So the contaminated parts of the plasmapause are not determined, causing gaps

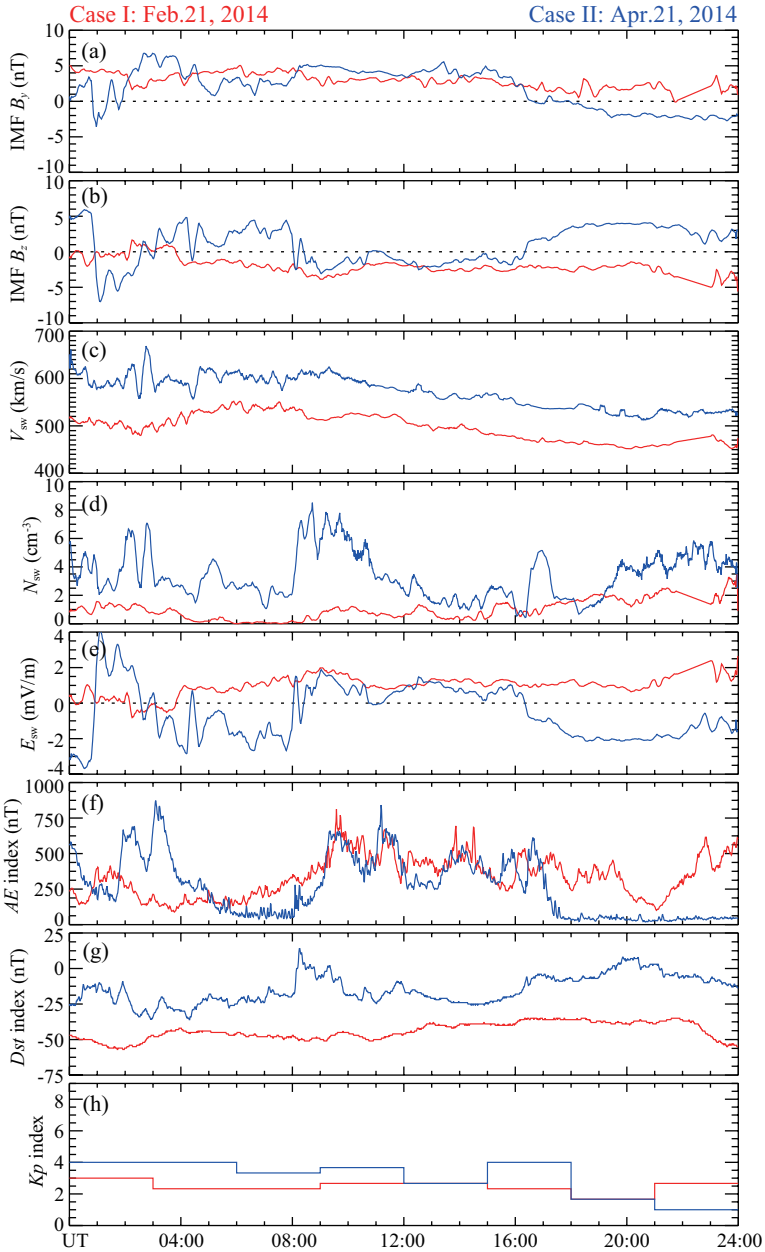

Figure 1. SW-IMF and geomagnetic conditions. The red curves are for Case I on 21 February 2014 and the blue curves are for Case II on 21 April 2014. The time shifted ACE SW-IMF data: B_y and B_z (in GSM), SW flow speed V_{SW}, SW electric field E_{SW}=-V_{SW}×B_z, and SW proton density N_{SW} are indicated in panels (a)-(e), and the *AE*, *Dst* and *Kp* indices are shown in panels (f)-(h), respectively.

in the curves in Figures 2 and 3.

The third step is to calculate the LOS vector in SM. The vector in SCS is calculated based on the pixel size of 0.25 mm and focal length of 150.0 mm for the EUVC, and then the vector is transformed to SM coordinate system using the matrix calculated in the first step.

The forth step is to calculate the *L* values of all the magnetic field lines intersected by the LOS in SM using the IGRF 2010 internal magnetic field model combined with the Tsyganenko 2007 external magnetic field model (Tsyganenko and Sitnov, 2007; Sitnov et al., 2008). The field line with the minimum *L* value is identified and the corresponding point on the SM equator is saved for a plasmapause location.

Finally, after all the plasmaspheric outline pixels are processed, a set of discrete plasmapause locations on the SM equator are interpolated with B-spline to form a smooth curve representing the equatorial plane plasmapause, as shown in Figures 2 and 3.

The EUVC was located between ~4.0 h and ~5.0 h MLT for Case I, and between ~5.0 h and ~6.0 h MLT for Case II, respectively, and all the images are projected in the yz plane of the Satellite Coordinate System (SCS) (He F et al., 2016). The EUVC data released by the National Astronomical Observatories are all projected onto the *yz* plane of the SCS. The *x* axis of SCS is pointed to the Earth (also the axis of the FOV of EUVC), the z axis of SCS is pointed to

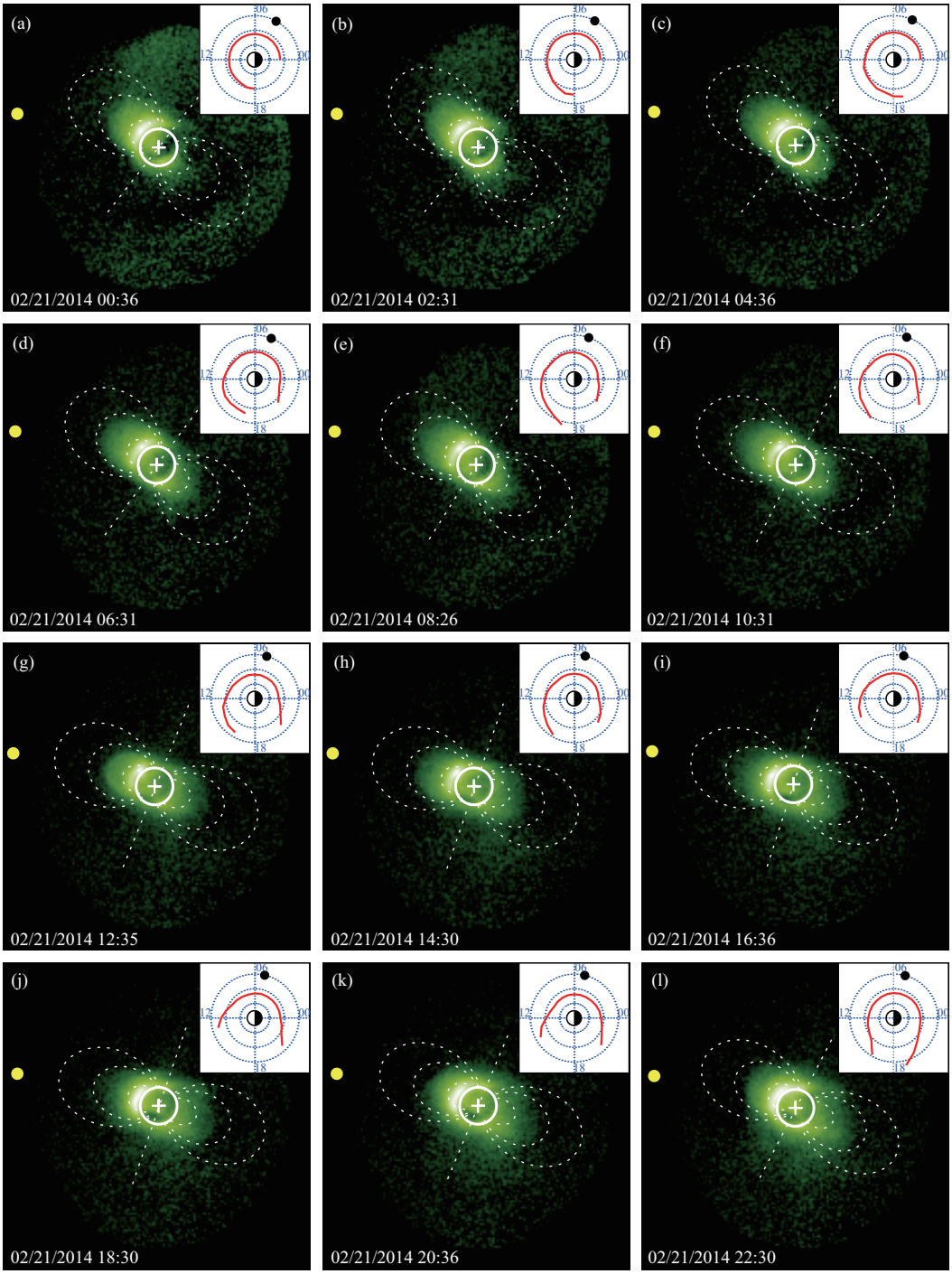

Figure 2. EUVC images for Case I on 21 February 2014. White crosses and circles represent the Earth, yellow dots represent the directions of the Sun, and white dashed straight lines represent the dipolar axis with up for north. White dashed curves represent the projections of the dipolar magnetic field lines with *L*-values of 2.0, 4.0 and 6.0 in the meridian planes perpendicular to the axis of the FOV of EUVC. Reconstructed magnetic equatorial plane plasmapause shape is shown at the upper right corner of each panel by red thick solid curves with noon to the left and dusk to the down and three blue dotted circles representing geocentric distances of 2.0 R_E, 4.0 R_E and 6.0 R_E, respectively. The black dots in the upper right of each corner represent the azimuthal direction of the EUVC.

the local north of the Moon, and the *y* axis is defined according to the right-hand law. In all the EUVC images displayed in this paper, the horizontal direction is from left to right along the SCS *y* axis, and the vertical direction is from down to up along the SCS *z* axis. It is noted that the SCS varies with the lunar motion. For each EUVC image, the unit vectors of the *x*, *y*, and *z* axes in SM coordinates system were calculated during the process of raw data. Then the vectors were included in the header of the released EUVC data files for users to calculate transformation matrix.

Figure 2 indicates that the overall size of the plasmasphere was re-

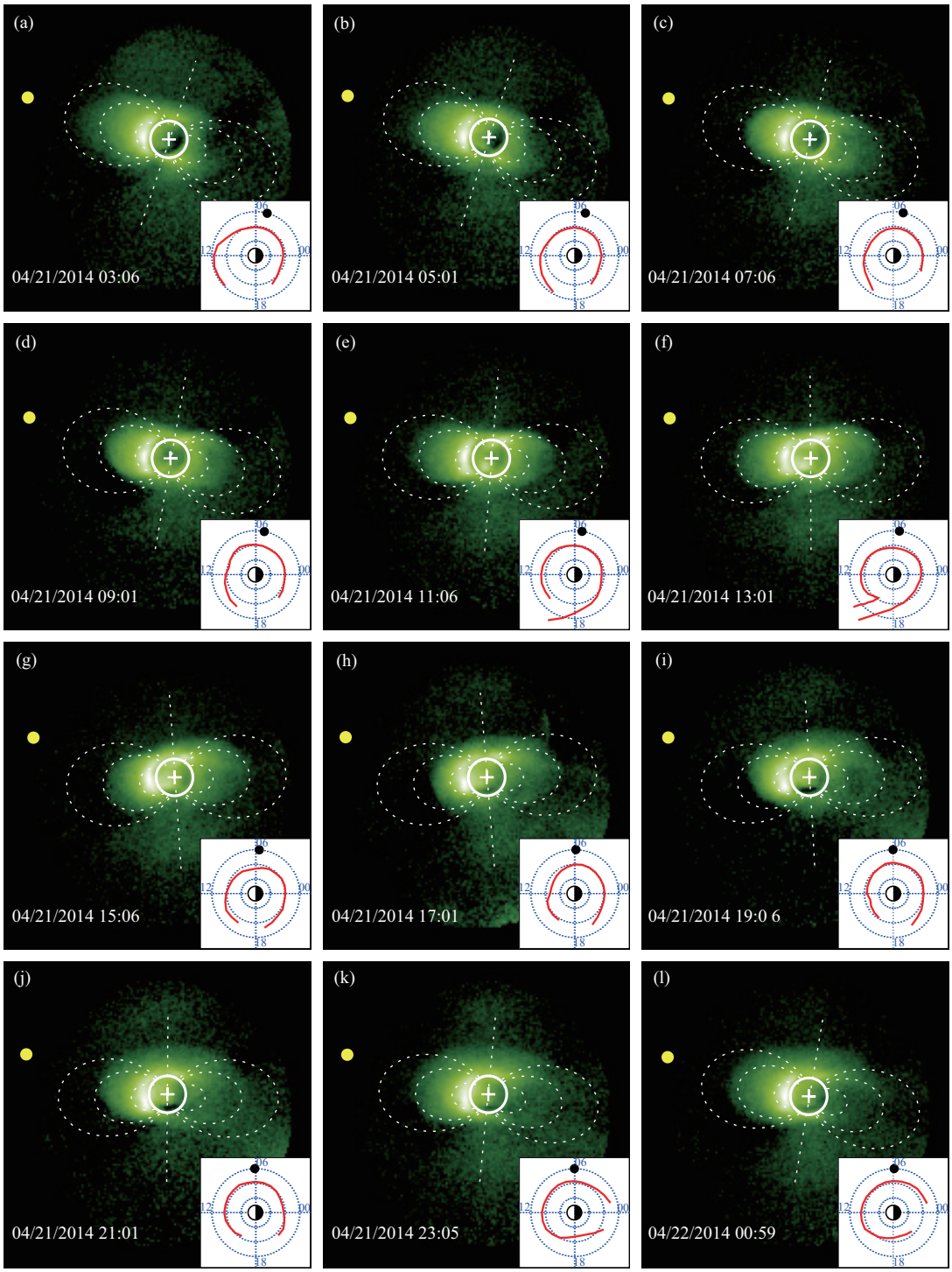

Figure 3. The same as Figure 2 but for Case II on 21 April 2014. Note that the reconstructed plasmapause shapes are shown at the lower right corners.

latively small for the whole day during which the plasmasphere was recovering from the moderate geomagnetic storm on 19-20 February. Continuous plasmaspheric refilling started from 00:36 UT till 06:31 UT (Figures 2a-2d), and the plasmapause expanded by approximately 0.5 R_E in 0 - 12 h MLT sector and by more than 1.0 R_E in 12 - 18 h MLT sector. The nightside plasmasphere was then eroded around 07:30 UT while the dayside plasmapause moved sunward, especially in the noon to dusk sector, and an unwrapped plume was finally formed at 22:30 UT in the dusk in Figure 2l.

It is clearly shown in Figure 2 that the plasmasphere shrank from 00:36 UT to 10:31 UT and expanded after 12:35 UT in the polar region (along the projected dipole axis), caused by the variations of the latitude of the EUVC in SM coordinate system and the generation of the unwrapped plume. Note that the distance of the EUVC to the SM equatorial plane changed from -21.85 R_E to -5.65 R_E

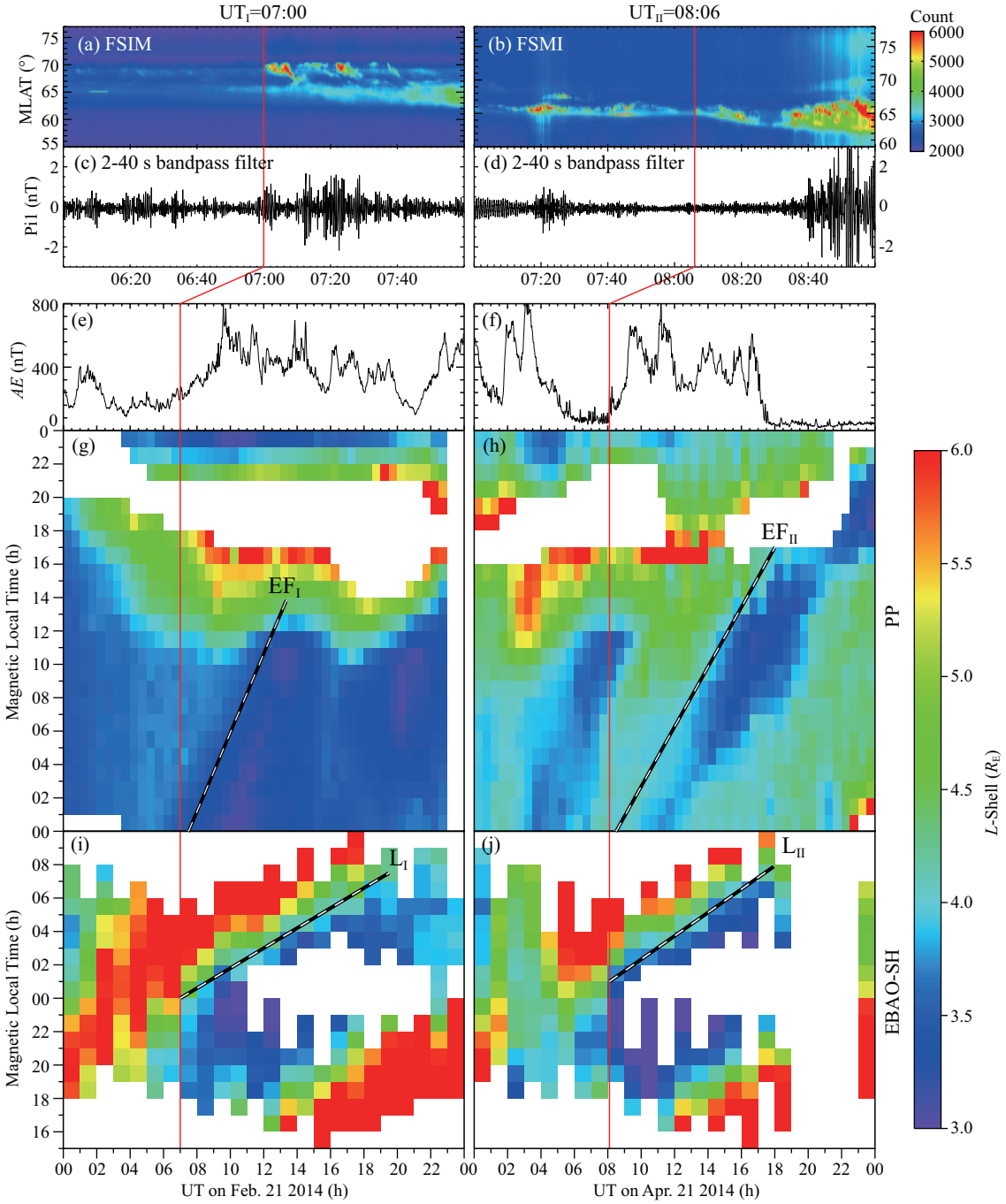

Figure 4. Determination of the substorm onset times and the evolutions of the plasmasphere and the aurora. Left is for Case I and right is for Case II. From top to bottom, shown are: auroral keograms taken from (a) Fort Simpson (FSIM) ASI on 21 February 2014 and (b) Fort Smith (FSMI) on 21 April 2014; Pi1 pulsations (2-40 s) calculated from the 0.5 s temporal resolution magnetometer data at (c) FSIM and (d) FSMI; (e-f) the *AE* index; (g-h) the keogram-style plot of the PP; (i-j) the keogram-style plot of the *L*-shell of the EBAO in southern hemisphere (SH), respectively. The red vertical lines represent substorm onsets at UT$_I$=07:00 and UT$_{II}$=08:06, and the dashed lines marked with EF$_I$ and EF$_{II}$ represent the two erosion fronts (EFs) of the plasmasphere, with L$_I$ and L$_{II}$ representing the expansion fronts of the auroral oval in SH, respectively. Note that same color bar is adopted for both the PP and the EBAO.

from 00:36 UT to 10:31 UT and changed from -5.65 R_E to -26.26 R_E after then. The closer the EUVC is to the SM equatorial plane, the narrower the plasmasphere is exhibited in the vertical direction of the images (e.g., Figure 3 in (He F et al. 2011)). Figure 2l indicates that the plume extended approximately along the vertical direction in the images when the longitudinal direction of the plume on the equatorial plane was approximately parallel to the axis of the FOV of EUVC (He F et al., 2013), resulting in expansion of the plasmasphere after 16:36 UT.

It is shown in Figure 3 that the first small scale erosion began at ~ 03:00 UT (Figure 3a) after the sudden enhancement of *AE* index at ~ 02:00 UT (Figure 1f), and the plasmasphere recovered until

08:00 UT (can be seen clearly in Figure 4h). Following the second erosion (Figure 3d) after the substorm began at ~08:00 UT, a wrapped plume was formed after ~09:00 UT and became the most apparent at 13:01 UT (Figure 3f). Then the plume started to corotate eastward around 17:00 UT as a result of the expansion of the corotation region due to the northward turning of the IMF shown in Figure 1. At about 23:05 UT, the plume had drifted to the midnight sector. This is consistent with Grebowsky's model (Grebowsky, 1970) that the plume just corotates and can move from dayside or dusk to nightside during weak convection or quiet time. It is worth noting that the nightside pointing plumes have been seldom reported and studied (Grebowsky, 1970; Ober et al., 1997b), and the generation of plumes at dusk sector and corotation of plumes to the midnight during less disturbed SW-IMF and/or geomagnetic periods needs further investigation.

4. Determination of Substorm Onset Times

To investigate the correlations between the plasmapause evolutions and the variations of auroral signatures during substorms, it is important to accurately determine the substorm onset times. The all sky imagers (ASI) and the magnetometers data from the Time History of Events and Macroscale Interactions during Substorms (THEMIS) Ground Based Observatories (GBO) (Wanliss, 2006; Mende et al., 2007; Zou S et al., 2010) were used to determine the timing of substorm onsets for these two cases, so as to investigate the correlations between the plasmaspheric evolutions and the substorm activities.

The keogram of the ASI auroral images with 3 seconds' cadence and the Pi1 pulsations (2-40s) calculated from the magnetometer data sampled at 2 Hz at Fort Simpson (FSIM) station (geographic latitude 61.8°, longitude 238.8°; magnetic latitude 67.3°) from 06:30 UT to 07:30 UT on 21 February 2014 are shown in Figures 4a and 4c, respectively. In both panels, the vertical dashed line indicates the substorm onset time at 07:00 UT located at ~70° magnetic latitude (MLAT) and 22.4 h MLT. After onset, the aurora expanded equatorward and kept disturbed until the end of the day. The auroral brightening was associated with significant Pi1 pulsations as shown in Figure 4c.

The keogram of the auroral images and corresponding Pi1 pulsations at Fort Smith (FSMI) station (geographic latitude 60.0°, longitude 248.2°; magnetic latitude 67.4°) for the substorm happeded after 08:00 UT on 21 April 2014 are shown in Figures 4b and 4d, respectively. The localized brightening of auroral from 07:16 to 08:00 in Figure 4b corresponded to the pseudobreakup event with no significant equatorward expansion of the aurora oval. After substorm onset at 08:06 UT located at ~65° MLAT and ~0.0 h MLT, the aurora brightened significantly and expanded both equatorward and poleward associated with significant Pi1 pulsations in Figure 4d especially after 08:30 UT.

5. Correlations Between Plasmaspheric Evolutions and Auroral Signature

The magnetic equatorial plasmapause (PP) locations are extracted from the EUVC images using the MLA. The auroral images at 135.6 nm obtained from the SSUSI onboard the DMSP satellites F16, F17 and F18 are mapped into a magnetic latitude-MLT grid in SM coordinate system. The equatorward boundary of auroral oval (EBAO) was extracted with the boundary recognition algorithm (Cao CG et al., 2009). Both the PPs and the EBAOs are extracted in 1 h MLT intervals when data are available. Since the time resolution for EUVC images is 10 min and the time intervals for DMSP passing the same hemisphere is 30 min to 1 h, the PPs are binned into 30 min intervals and the EBAOs are binned to 1 h intervals to ensure the continuity in UT. Figures 4e-4j show the evolutions of the *AE* index, the geocentric distances of the magnetic equatorial plasmapause (PP), the MLAT of the EBAO in the southern hemisphere for Case I (left) and Case II (right), respectively. Note that we are not going to focus on the white portion in Figures 4g-4j where no plasmapause location is determined from the EUVC images and/or no EBAO extracted from the DMSP SSUSI auroral images.

Two significant erosions of the plasmasphere are shown in Figures 4g and 4h with the substorm onset times labeled with UT_I=07:00, and UT_{II}=08:06 as determined in previous section, respectively. The most important features in Figures 4g and 4j are that erosions of the plasmasphere are highly correlated with auroral activities. The thick dashed lines defined as "erosion front" (EF) in Figures 4g and 4h represent the time (UT) and position (MLT) at which the plasmaspheric erosions began. In both cases, the onsets of the substorms began at midnight sector between ~21.0 h and ~1.0 h MLT as indicated by the thick dashed lines in Figures 4i and 4j. Then the auroral oval expanded equatorward and propagated eastward from midnight to dawn. The lines L_I and L_{II} were obtained by fitting the UT at which the auroral oval began expansion to the MLT. Similar eastward propagation trends are found in the plasmaspheric erosions as indicated by the EFs with speeds of 2.17 MLT/h and 1.89 MLT/h in Figures 4g and 4h, respectively. It is noted that after substorm onsets, the dayside plasmapause began to move sunward and the dayside EBAO moved towards high latitudes. When the nightside plasmaspheric erosions propagated to the dayside, the dayside plasmapause began erosion too. It is also indicated that the plasmaspheric erosions were apparently modulated by the auroral activities during the substorms since the solar-wind-driven convections were very weak for these two cases as shown in Figure 1.

6. Discussion

In this paper, we have reported nightside pointing plume which drifted from the dusk sector observed by CE-3 EUVC on 21 April 2014. Several similar nightside pointing plumes were also found in IMAGE EUV images under quiet SW-IMF and geomagnetic activities. This substantial observation of nightside pointing plumes during quiet and less disturbed SW-IMF and geomagnetic conditions ($|E_{SW}|$ < 2 mV/s, *AE* < 50 nT, *Kp* < 2, and *Dst* > -10 nT) is different from the traditional large-scale convection theory of the plasmasphere (Chen AJ and Wolf, 1972; Rasmussen et al., 1993) and has seldom been reported in the literature.

High correlations between the plasmapause evolutions and the auroral signatures during substorms based on CE-3 EUVC and DMSP SSUSI observations were also found. During the two substorms studied, the plasmapause erosions began at the substorm

onsets around midnight, and then the erosion propagated towards morning side. The tendency of the plasmaspheric erosions was consistent with the equatorward expansion of the auroral oval. When the equatorial boundaries of the auroral oval are mapped onto the magnetic equatorial plane, the averaged *L*-values of the boundary around the line L_I and L_{II} are ~ 4.0 R_E and ~ 4.3 R_E with the corresponding averaged *L*-values of the plasmapause location around the line EF_I and EF_{II} to be ~3.5 R_E and ~3.9 R_E for Case I and Case II, respectively. This implies that the auroral equatorward boundary approximately matches the plasmaspheric erosion front location. A possible interpretation of such correlations is as follows.

Before substorm onsets, the geomagnetic field in the magnetotail is stretched and energy is stored in the magnetotail. It is commonly noted that southward turning of IMF triggered the dissipation of magnetotail energy which is injected into the auroral region and initiated the substorm growth phases. In dissipation of the magnetotail energy, geomagnetic field has changed to more dipolar configuration, and the dipolarization front is formed first in the premidnight-midnight sector, and then moves towards the Earth and spreads both eastward and westward (Runov et al., 2009; Ohtani et al., 1992). At the same time, substorm dipolarization causes pitch-angle scattering of plasma sheet electrons and the resulting precipitation excites auroral emissions. On the other hand, enhanced convection during substorms or dipolarization fronts produces plasmaspheric erosions. Therefore, we suggest that the substorm dipolarization is closely associated with plasmaspheric erosions, the propagation of EFs, and the corresponding electron pitch-angle scattering causing the auroral signatures during substorms.

Preliminary investigation in this work indicates that the dynamics of the plasmasphere and ionosphere are strongly dependent on internal processes of the magnetosphere when solar wind-driven convections are weak and steady. More works including simulations need to be done in future to further understand the mechanism of generating the nightside pointing plumes and the inner magnetospheric dynamics during substorms. For example, wave induced scattering and field line curvature scattering might also drive the DMSP observed auroral activity. More cases with global auroral images and global plasmaspheric images should be collected to systematically study the relationship between the auroral activity and the plasmaspheric dynamics during substorms in future.

Acknowledgements

The authors are grateful to EUVC development team at Changchun Institute of Optics, Fine Mechanics and Physics (CIOMP), Chinese Academy of Sciences, and the Ground Application System of the Chinese Lunar Exploration Program at the National Astronomical Observatories (NAO), Chinese Academy of Sciences, for the provision of the CE-3 EUVC data. The THEMIS GBO-s ASI and magnetometer data are provided by UC Berkeley available from http://themis.ssl.berkeley.edu/index.shtml [2014-04-21] and we acknowledge the PIs and investigators for these instruments as listed on this website. We thank T. Forrester of IMAGE EUV team for provision of the EUV data and relevant processing software. The SW-IMF data are provided by NOAA available from http://www.swpc.noaa.gov/products/ace-real-time-solar-wind[2014-04-21). The *Dst* and *AE* indices are provided by the Kyoto World Data Center for Geomagnetism available from http://wdc.kugi.kyoto-u.ac.jp/[2014-04-21) . The *Kp* index is provided by the German Research Centre for Geosciences (GFZ). The authors would like to thank NASA-CCMC and N. A. Tsyganenko for providing the code of IGRF and Tsyganenko model. This work was supported by National Natural Science Foundation of China (41674155 and 41274147), Youth Innovation Promotion Association of Chinese Academy of Sciences (No. 2017258) and Key Research Project of Chinese Academy of Sciences: Application Research on the Scientific Data from Chang'E-3 Mission (KGZD-EW-603).

References

Akasofu, S. I. (1964). The development of the auroral substorm. *Planet. Space Sci.*, *12*, 273-282. https://doi.org/10.1016/0032-0633(64)90151-5

Burch, J. L. (2003), Magnetospheric Imaging – The Image Prime Mission, Kluwer Academic Publishers, Dordrecht..

Cao, C. G., Newman, T. S., and Germany,G. A. (2009). New shape-based auroral oval segmentation driven by LLS-RHT. *Pattern Recogn.*, *42*, 607-618. https://doi.org/10.1016/j.patcog.2008.08.018

Carpenter, D. L., and A. J. Smith (2001). The study of bulk plasma motions and associated electric fields in the plasmasphere by means of whistler-mode signals. *J. Atmos. Solar-Terr. Phys.*, *63*, 1117-1132. https://doi.org/10.1016/S1364-6826(00)00217-0

Chen, A. J., and Grebowsky, J. M. (1974). Plasma tail interpretations of pronounced detached plasma regions measured by Ogo 5. *J. Geophys. Res.*, *79*, 3851-3855. https://doi.org/10.1029/JA079i025p03851

Chen, A. J., and Wolf, R. A. (1972). Effects on the plasmasphere of a time-varying convection electric field. *Planet. Space Sci.*, *20*, 483-509. https://doi.org/10.1016/0032-0633(72)90080-3

Chen, B., Song, K. F., Li, Z. H., Wu, Q. W., Ni, Q. L., Wang, X. D., Xie, J. J., Liu, S. J., He, L. P., He, F., Wang, X. G., Chen, B., Zhang, H. J., Wang, X. D., Wang, H. F., Zheng, X., E, S. L., Wang, Y. C., Yu, T., Sun, L., Wang, J. L., Wang, Z., Yang, L., Hu, Q. L., Qiao, K., Wang, Z. S., Yang, X. W., Bao, H. M., Liu, W. G., Li, Z., Chen, Y., Gao, Y., Sun, H., and Chen, W. C. (2014). Development and calibration of the Moon-based EUV camera for Chang'e-3. *Res. Astron. Astrophys.*, *14*, 1654-1663. https://doi.org/10.1088/1674-4527/14/12/013

Darrouzet, F., De Keyser, J., Décréau, P. M. E., El Lemdani-Mazouz, F., and Vallières, X. (2008). Statistical analysis of plasmaspheric plumes with CLUSTER/WHISPER observations. *Ann. Geophys.*, *26*, 2403-2417. https://doi.org/10.5194/angeo-26-2403-2008

Darrouzet, F., Gallagher, D. L., André， N., Carpenter, D. L., Dandouras, I., Décréau, P. M. E., De Keyser, J., Denton, R. E., Foster, J. C., Goldstein, J., Moldwin, M. B., Reinisch, B. W., Sandel, B. R., and Tu, J. N. (2009). Plasmaspheric density structures and dynamics: Properties observed by the CLUSTER and IMAGE missions. *Space Sci. Rev.*, *145*, 55-106. https://doi.org/10.1007/s11214-008-9438-9

Feng, J. Q., Liu, J. J., He, F., Yan, W., Ren, X., Tan, X., He, L. P., Chen, B., Zuo, W., Wen, W. B., Su, Y., Zou, Y. L., and Li, C. L. (2014). Data processing and initial results from the CE-3 Extreme Ultraviolet Camera. *Res. Astro. Astrophys.*, *14*, 1664-1673. https://doi.org/10.1088/1674-4527/14/12/014

Ge, Y. S., Zhou, X.-Z., Liang, J., Raeder, J., Gilson, M. L., Donovan, E., Angelopoulos, V., and Runov, A. (2012). Dipolarization fronts and associated auroral activities: 1. Conjugate observations and perspectives from global MHD simulations. *J. Geophys. Res.*, *117*(A10), A10226. https://doi.org/10.1029/2012JA017676

Goldstein, J., Sandel, B. R., Forrester, W. T., and Reiff, P. H. (2003a). IMF-driven plasmasphere erosion of 10 July 2000. *Geophys. Res. Lett.*, *30*, 1146. https://doi.org/10.1029/2002GL016478

Goldstein, J., Sandel, B. R., Hairston, M. R., and Reiff, P. H. (2003b). Control of plasmaspheric dynamics by both convection and sub-auroral polarization

stream. *Geophys. Res. Lett.*, *30*, 2243. https://doi.org/10.1029/2003GL018390

Goldstein, J., Sandel, B. R., Thomsen, M. F., Spasojević, M., and Reiff, P. H. (2004). Simultaneous remote sensing and in situ observations of plasmaspheric drainage plumes. *J. Geophys. Res.*, *109*(A3), A03202. https://doi.org/10.1029/2003JA010281

Goldstein, J., Burch, J. L., Sandel, B. R., Mende, S. B., C:son Brandt, P., and Hairston, M. R. (2005). Coupled response of the inner magnetosphere and ionosphere on 17 April 2002. *J. Geophys. Res.*, *110*(A3), A03205. https://doi.org/10.1029/2004JA010712

Goldstein, J., Sandelm, B. R., Frey, H. U., and Mende, S. B. (2007). Multiple plasmapause undulations observed by the IMAGE satellite on 20 March 2001. *J. Atmos. Solar-Terr. Phys.*, *69*, 322-333. https://doi.org/10.1016/j.jastp.2006.08.010

Goldstein, J., Thomsen, M. F., and DeJong, A. (2014). In situ signatures of residual plasmaspheric plumes: Observations and simulation. *J. Geophys. Res.*: *Space Phys.*, *119*, 4706-4722. https://doi.org/10.1002/2014JA019953

Grebowsky, J. M. (1970). Model study of plasmapause motion. *J. Geophys. Res.*, *75*, 4329-4333. https://doi.org/10.1029/JA075i022p04329

He, F., X. Zhang, X., Chen, B., and Fok, M.-C. (2011). Reconstruction of the plasmasphere from Moon-based EUV images. *J. Geophys. Res.*, *116*(A11), A11203. https://doi.org/10.1029/2010JA016364

He, F., Zhang, X. X., Chen, B., and Fok, M.-C. (2012a). Plasmaspheric trough evolution under different conditions of subauroral ion drift. *Sci. China Tech. Sci.*, *55*, 1287-1294. https://doi.org/10.1007/s11431-012-4781-1

He, F., Zhang, X. X., Chen, B., and Fok, M.-C. (2012b). Inversion of the Earth's plasmaspheric density distribution from EUV images with genetic algorithm. *Chinese J. Geophys.* (*in Chinese*), *55*, 29-35. https://doi.org/10.6038/j.issn.0001-5733.2012.01.003

He, F., Zhang, X.-X., Chen, B., Fok, M.-C., and Zou, Y.-L. (2013). Moon-based EUV imaging of the Earth's Plasmasphere: Model simulations. *J. Geophys. Res.*: *Space Phys.*, *118*, 7085-7103. https://doi.org/10.1002/2013JA018962

He, F., Zhang, X.-X., Chen, B., Fok, M.-C., and Nakano, S. (2016). Determination of the Earth's plasmapause location from the CE-3 EUVC images. *J. Geophys. Res.*: *Space Phys.*, *121*, 296-304. https://doi.org/10.1002/2015JA021863

He, H., Shen, C., Wang, H. N., Zhang, X. X., Chen, B., Yan, J., Zou, Y. L., Jorgensen, A. M., He, F., Yan, Y., Zhu, X. S., Huang, Y., and Xu, R. L. (2016). Response of plasmaspheric configuration to substorms revealed by Chang'E 3. *Sci. Rep.*, *6*, 32362. https://doi.org/10.1038/srep32362

Kwon, H.-J., Kim, K.-H., Jee, G., Park, J.-S., Jin, H., and Nishimura, Y. (2015). Plasmapause location under quiet geomagnetic conditions (Kp≤1): THEMIS observations. *Geophys. Res. Lett.*, *42*, 7303-7310. https://doi.org/10.1002/2015GL066090

Lemaire, J. F., Gringauz, K. I., Carpenter, D. L., and Bassolo, V. (1998), The Earth's Plasmasphere, Cambridge University Press, New York..

McPherron, R. L., Russell, C. T., and Aubry, M. P. (1973). Satellite studies of magnetospheric substorms on August 15, 1968: 9. Phenomenological model for substorms. *J. Geophys. Res.*, *78*, 3131-3149. https://doi.org/10.1029/JA078i016p03131

Mende, S. B., Angelopoulos, V., Frey, H. U., Harris, S., Donovan, E., Jackel, B., Syrjaesuo, M., Russell, C. T., and Mann, I. (2007). Determination of substorm onset timing and location using the THEMIS ground based observatories. *Geophys. Res. Lett.*, *34*, L17108. https://doi.org/10.1029/2007GL030850

Moldwin, M. B., Howard, J., Sanny, J., Bocchicchio, J. D., Rassoul, H. K., and Anderson, R. R. (2004). Plasmaspheric plumes: CRRES observations of enhanced density beyond the plasmapause. *J. Geophys. Res.*, *109*(A5), A05202. https://doi.org/10.1029/2003JA010320

Ober, D. M., Horwitz, J. L., and Gallagher, D. L. (1997a). Formation of density troughs embedded in the outer plasmasphere by subauroral ion drift events. *J. Geophys. Res.*, *102*(A7), 14595-14602. https://doi.org/10.1029/97JA01046

Ober, D. M., Horwitz, J. L., Thomsen, M. F., Elphic, R. C., McComas, D. J., Belian, R. D., and Moldwin, M. B. (1997b). Premidnight plasmaspheric "plumes". *J. Geophys. Res.*, *102*(A6), 11325-11334. https://doi.org/10.1029/97JA00562

Ohtani, S., Kokubun, S., and Russell, C. T. (1992). Radial expansion of the tail current disruption during substorms: A new approach to the substorm onset region. *J. Geophys. Res.*, *97*(A3), 3129-3136. https://doi.org/10.1029/91JA02470

Paxton, L. J., C. Meng, I., Fountain, G. H., Ogorzalek, B. S., Darlington, E. H., Gary, S. A., Goldsten, J. O., Kusnierkiewicz, D. Y., Lee, S. C., Linstrom, L. A., Maynard, J. J., Peacock, K., Persons, D. F., and Smith, B. E. (1992). Special sensor ultraviolet spectrographic imager (SSUSI): An instrument description. *Pro. SPIE*, *1745*, 2. https://doi.org/10.1117/12.60595

Pierrard, V., and Lemaire, J. F. (2004). Development of shoulders and plumes in the frame of the interchange instability mechanism for plasmapause formation. *Geophys. Res. Lett.*, *31*, L05809. https://doi.org/10.1029/2003GL018919

Rasmussen, C. E., Guitar, S. M., and Thomas, S. G. (1993). A two-dimensional model of the plasmasphere: Refilling time constants. *Planet. Space Sci.*, *41*, 35-43. https://doi.org/10.1016/0032-0633(93)90015-T

Runov, A., Angelopoulos, V., Sitnov, M. I., Sergeev, V. A., Bonnell, J., McFadden, J. P., Larson, D., Glassmeier, K.-H., and Auster, U. (2009). THEMIS observations of an earthward-propagating dipolarization front. *Geophys. Res. Lett.*, *36*, L14106. https://doi.org/10.1029/2009GL038980

Sandel, B. R., Broadfoot, A. L., Curtis, C. C., King, R. A., Stone, T. C., Hill, R. H., Chen, J., Siegmund, O. H. W., Raffanti, R., Allred, D. D., Turley, R. S., and Gallagher, D. L. (2000). The extreme ultraviolet imager investigation for the image mission. *Space Sci. Rev.*, *91*, 197-242. https://doi.org/10.1023/A:1005263510820

Sandel, B. R., King, R. A., Forrester, W. T., Gallagherm, D. L., Broadfoot, A. L., and Curtis, C. C. (2001). Initial results from the IMAGE extreme ultraviolet imager. *Geophys. Res. Lett.*, *28*, 1439-1442. https://doi.org/10.1029/2001GL012885

Sandel, B. R., Goldstein, J., Gallagher, D. L., and Spasojević, M. (2003). Extreme ultraviolet imager observations of the structure and dynamics of the plasmasphere. *Space Sci. Rev.*, *109*, 25-46. https://doi.org/10.1023/B:SPAC.0000007511.47727.5b

Sitnov, M. I., Tsyganenko, N. A., Ukhorskiy, A. Y., and Brandt, P. C. (2008). Dynamical data-based modeling of the storm-time geomagnetic field with enhanced spatial resolution. *J. Geophys. Res.*, *113*(A7), A07218. https://doi.org/10.1029/2007JA013003

Spasojević, M., Goldstein, J., Carpenter, D. L., Inan, U. S., Sandel, B. R., Moldwin, M. B., and Reinisch, B. W. (2003). Global response of the plasmasphere to a geomagnetic disturbance. *J. Geophys. Res.*, *108*(A9), 1340. https://doi.org/10.1029/2003JA009987

Spasojević, M., Frey, H. U., Thomsen, M. F., Fuselier, S. A., Gary, S. P., Sandel, B. R., and Inan, U. S. (2004). The link between a detached subauroral proton arc and a plasmaspheric plume. *Geophys. Res. Lett.*, *31*, L04803. https://doi.org/10.1029/2003GL018389

Tsyganenko, N. A., and Sitnov, M. I. (2007). Magnetospheric configurations from a high-resolution data-based magnetic field model. *J. Geophys. Res.*, *112*(A6), A06225. https://doi.org/10.1029/2007JA012260

Walsh, B. M., Phan, T. D., Sibeck, D. G., and Souza, V. M. (2014). The plasmaspheric plume and magnetopause reconnection. *Geophys. Res. Lett.*, *41*, 223-228. https://doi.org/10.1002/2013GL058802

Wang, C. L., Newman, T. S., and Gallagher, D. L. (2007). Plasmapause equatorial shape determination via the Minimum L Algorithm: Description and evaluation. *J. Geophys. Res.*, *112*(A12), A12201. https://doi.org/10.1029/2006JA012202

Wanliss, J. (2006). Substorm onset location and dipole tilt angle. *Ann. Geophys.*, *24*, 577-588. https://doi.org/10.5194/angeo-24-577-2006

Yan, Y., Wang, H. N., He, H., Chen, B., Feng, J. Q., Ping, J. S., Shen, C., Xu, R. L., and Zhang, X. X. (2016). Analysis of observational data from Extreme Ultra-Violet Camera onboard Chang'E-3 mission. *Astrophys. Space Sci.*, *361*, 76. https://doi.org/10.1007/s10509-016-2650-2

Zhang, X. X., Wang, C., Chen, T., Wang, Y. L., Tan, A., Wu, T. S., Germany, G. A., and Wang, W. (2005). Global patterns of Joule heating in the high-latitude ionosphere. *J. Geophys. Res.*, *110*(A12), A12208. https://doi.org/10.1029/2005JA011222

Zou, S., Moldwin, M. B., Lyons, L. R., Nishimura, Y., Hirahara, M., Sakanoi, T., Asamura, K., Nicolls, M. J., Miyashita, Y., Mende, S. B., and Heinselman, C. J. (2010). Identification of substorm onset location and preonset sequence using Reimei, THEMIS GBO, PFISR, and Geotail. *J. Geophys. Res.*, *115*(A12), A12309. https://doi.org/10.1029/2010JA015520